

Icephobicity and Electrical Assessment of Slippery Coating Impregnated with a Stabilized Hydroxyl-Terminated Lubricant for High Voltage Insulation Application

Samaneh Heydarian^{1*}, Gelareh Momen¹ and Reza Jafari¹

¹Department of Applied Sciences, University of Québec at Chicoutimi (UQAC), 555, boul. de l'Université,
Chicoutimi, Québec, G7H 2B1, Canada

*Corresponding author: samaneh.heydarian-dolatabadi1@uqac.ca

Abstract

In cold climate conditions, insulators are subjected to ice accretion that could affect their electrical performance and consequently lead to power outages. Besides icing, other outdoor factors, such as UV, rain, and pollution, could influence their electrical insulation efficiency. Slippery liquid-infused coatings have attracted great attention due to their icephobic applications. However, the problems caused by lubricant depletion could restrict their service time and thus limit their applications. Here, lubricant-loaded carrier (LLC) powders were first, obtained by applying negative pressure through a three-step procedure. Then, hydroxyl-terminated silicone oil carriers were impregnated into a blend of polydimethylsiloxane (PDMS) and alkoxy-siloxane resin. The fabricated coatings exhibited long-lasting icephobic characteristics, resulting in reduced amount of ice accumulated on the surfaces. This reduction in ice adhesion is related not only to the slippery behavior of the coatings but also the formation of unfrozen hydrogen-bonded

molecules. The coatings exhibited desired stability against weathering conditions, such as UV exposure and humidity. The electrical characteristics of the prepared coatings were evaluated using dielectric spectroscopy, flashover, condensation, and inclined plane tests. Accordingly, the coatings containing lubricant-loaded carriers showed increased flashover voltage in dry, wet, and polluted states and reduced leakage currents in the condensation test.

Keywords: Icephobic surfaces, slippery coatings, hydroxyl-terminated silicone oil, high voltage insulator, leakage current, flashover

1. Introduction

Ice formation and accumulation could cause catastrophic blackouts in a wide range of settings, particularly power transmission and distribution [1, 2]. The adhesion of ice on insulators, as an essential part of transmission lines, is also considered as a devastating economical and safety issue during ice storms in cold climate regions [3]. Such components are used to provide mechanical support for electrical components and separate high-voltage line conductors. Besides ice accretion, the presence of pollution layer, including soluble mineral substances, on insulators could affect their electrical performance [4]. In fact, the migration of these contaminations towards the uppermost layer of ice could change the accumulated ice into highly conductive matter, resulting in further leakage current. Consequently, this causes formation of conductive water layer on the surface, leading to flashover. Other issues, including thermal degradation, corona discharge, and dry band arcing, are among the factors that result in electrical failure [5].

Various preventative strategies have been used to remove ice and pollution from the insulator surface. These strategies included change in insulator substance, shape, dimension and applying grease as a de-icing material [6, 7]. However, most of them were ineffective, and therefore, much work has been focused on modifying the surface characteristics of insulators that are mostly gloss- and porcelain-based [8].

Hydrophobic coatings based on room-temperature-vulcanizing (RTV) silicone rubber were among the pioneer generations that were applied on glass and porcelain insulators [9–13]. They were chosen due to their water repellency characteristics and suitable long-term performance under conditions of road salt and industrial pollution [14–17]. However, they were not effective at harsh icing circumstances due to loss of hydrophobicity, resulting in increased discharge current. Semiconductive silicone coatings containing conducting particles, such as zinc oxide and graphene oxide (GO), were also proposed to be applied on insulators that offered enhanced anti-icing performance [18–21]. However, they had some drawbacks, such as high-power loss, aging, and degradation [22–24]. Superhydrophobic coatings have also shown some promising results for being applied on insulators [25–30]. These coatings present high-water repellency that could result in decreased ice accretion over insulators. Despite their optimized icephobic effectiveness, using superhydrophobic coatings demonstrated some disadvantages that limit their applications, particularly exposure to harsh environmental conditions, such as high humidity that much likely leads to losing their anti-icing characteristics [31–33]. Under such condition, water molecules condense in the porous surface structure that promotes mechanical interlocking between ice and the surface and consequently increase ice adhesion.

By imitating the morphology of *Nepenthes* pitcher plants, slippery liquid-infused porous surfaces (SLIPS) have been developed, and they do not have issues related to water condensation in high-humidity conditions [34–36], due to replacing air by oil within the surface pores. Infusing a lubricant into the porous substrate produces a smooth surface with fewer pinning points that exhibits low contact hysteresis and tilted angle [37–39]. Polymer-based SLIPS are generally fabricated by infusing lubricant in either a preformed structure or a precursor matrix [39–41]. Having greater control on composition in the latter method could prevent swelling deformation of the matrix.

SLIPS have shown high potential to be used in a wide range of applications, including anticorrosion, biomedical, and icephobic needs [43–47]. Aizenberg's group designed SLIPS by infusing a perfluorinated lubricant into a micro/nanostructured surfaces [34]. Besides low contact-angle hysteresis and low sliding angles, the fabricated coatings showed excellent ice-repellency characteristics. Golovin et al. investigated the effect of lubricant being infused on the stiffness of polymeric matrices and proposed the concept of interfacial slippage [48, 49]. Accordingly, the combination of elasticity and the presence of lubricating layer could result in ice adhesion strength of lower than 20 kPa. In another attempt, SLIPS was fabricated by infusing liquid paraffin into polymethylsiloxane (PDMS), exhibiting a very low ice adhesion strength of 1.7 kPa at $-30\text{ }^{\circ}\text{C}$ [50].

Due to the extraordinary icephobic characteristics of SLIPS, they could be considered as a suitable candidate to prevent ice accretion on insulators and thus electrical failure. Wang et al. prepared silicone-oil-infused PDMS coating with different lubricant contents and evaluated the ice accumulation of coated insulator in high voltage chamber. The low surface energy of the lubricant and PDMS and the high mobility of the silicone oil within

the matrix network could effectively contribute in reducing the ice adhesion strength on the insulator coated with the fabricated coatings [51]. Olad et al. developed SLIPS coatings by infusing perfluorinated lubricants into two different chemically modified porcelain substrates. The fabricated surfaces exhibited acceptable ice repellency properties, and they endured inclined plane test (IPT) at 4.5 kV for 6 h [52].

Given that oil is one of the essential components of SLIPS to have desirable icephobic properties, lubricant loss could result in limited service life and consequently restrict their applications [53]. Therefore, stabilizing the oil in the matrix structure to lengthen service life has become one of the main challenges in the fabrication of slippery coatings. Accordingly, some methods, such as using nanoparticles and nano-porous materials and micro-texturing, have been proposed [54–56]. These strategies for lubricant retention in slippery coatings were not used in most relevant studies regarding the fabrication of such coatings for electrical applications.

In this work, a slippery lubricant infused coating that contained silica-based carriers was developed to enhance the coating's durability. First, hydroxy-terminated silicone oil was infused into the silica aerogel pores by applying negative pressure to obtain lubricant-loaded carrier (LLC) powders. Then, the fabricated powders were impregnated in silicone-based blend. The icephobic characteristics of the prepared coatings were evaluated using different test methods, including DSC, micro-push-off adhesion test, push-off test, and static accumulation test (SAT). The weathering resistance of the coatings were assessed using QUV. A comprehensive group of electrical tests, namely, dielectric spectroscopy, flashover and condensation test, and IPT, was also conducted. The findings showed that

the fabricated coatings containing lubricant-loaded carriers could be a suitable potential candidate for application on insulators.

2. Materials and methods

2.1. Fabrication of coatings containing lubricant-loaded carriers

The preparation of the coatings consisted of two general procedures, namely, loading the lubricant inside the carriers and impregnating lubricant-loaded carriers within the matrix. In the former procedure, hydroxyl-terminated silicone oil (Genesee Polymers), with a viscosity of 100 cSt and molecular weight of 3400 amu, was loaded into the hydrophobic silica aerogel (particle size of 2–40 μm , Enova Aerogel IC3100). To increase the loading capacity and stabilize lubricant within the aerogel's micropores, the following three-step procedure was conducted through applying negative pressure. First, 0.1 g of aerogel was mixed with 10 g of a prepared solution of the oil in hexane (60 wt.%). After 10 min of sonicating, the prepared dispersion was then, vacuumed at 60 kPa at 40 °C for 1 h. This process was repeated three times to further infuse the oil within the carrier pores. Finally, the powder-like lubricant-loaded carriers were obtained after the mixture was washed with hexane and dried for 24 h at 60 °C. The loading capacity of the carriers was evaluated using thermogravimetric analysis (TGA, Netzsch STA 449C).

The coatings were fabricated by embedding the prepared lubricant-loaded carriers within a blend of polydimethylsiloxane (PDMS) and alkoxy-siloxane resin. For this purpose, PDMS (Sylgard 184 silicone elastomer) serving as a base and a curing agent was mixed with the alkoxy-siloxane resin (DOWSIL 2405) at a ratio of 70:30, respectively. This ratio was selected based on the hardness measurement described in supplementary Figure S1. Furthermore, the SEM micrograph of the matrix with mentioned combination showed no

evidence of immiscibility (see supplementary Figure S2). According to the data sheet, the alkoxy-siloxane resin could act as a co-binder that enhances the mechanical performance of silicone-based coatings. Different percentages (5 wt.%, 10 wt.%, and 15 wt.%) of the lubricant-loaded carriers, dispersed in suitable amount of xylene, were added into the prepared polymeric blend. The curing agent of PDMS was added to the mixture (ratio of 1:10), and tetraethoxysilane (TEOS, Dow Corning) as a coupling agent of alkoxy-siloxane resin. Aluminum plates polished by 800 and 1200 SiC papers were used as the substrate. After 10 min of stirring, each mixture was applied on the treated substrate by using a film applicator (ZEHNTER testing instrument). The coated samples were then placed in the oven overnight at 90 °C to complete their curing process. The samples were labeled on the basis of the content of lubricant-loaded carriers as LLC-5, LLC-10, and LLC-15; for instance, sample LLC-10 contained 10 wt.% of LLC. Furthermore, the polymeric sample without LLC was selected as a reference. The average thickness of the carried coatings was around $100 \pm 5 \mu\text{m}$, measured by a coating thickness gauge. The micrographs of LLCs and cross-section of the coating containing LLCs were provided in supplementary figure S3, depicting their size and spatial distribution.

2.2. Surface characterization

The water contact angle was measured using a Kruss DSA100 goniometer at 25 °C, based on the Young-Laplace approximation. A 4 μL deionized water droplet was placed onto the sample surface to determine the contact angle. The contact angle hysteresis was obtained by measuring the difference between the advancing and receding contact angles when the water droplet was moved by the needle across the sample surface. The measurement was repeated at three different points of each sample to ensure its accuracy. An optical profiler

(Profil3D, Filmetrics, USA) was used to evaluate the topography of the samples and quantify the corresponding surface parameters.

2.3. Icephobic properties

The delayed ice nucleation temperature of the prepared samples was obtained by DSC. In this procedure, a 5 mg-deionized water droplet was placed into an aluminum DSC pan that had already been coated by each coating. After being sealed, the pan was placed on a DSC sample holder, and the measurement was conducted by cooling down the sample from 40 to $-40\text{ }^{\circ}\text{C}$ with a ramp of $5\text{ }^{\circ}\text{C}/\text{min}$.

The ice adhesion strength of the fabricated coatings in micro and macro scales was evaluated using micro-push-off and push-off tests. In the micro-push-off test, a $10\text{ }\mu\text{L}$ deionized water was deposited on a cooling plate located in a small cold chamber at $-10.0\text{ }^{\circ}\text{C} \pm 0.1\text{ }^{\circ}\text{C}$ and under relative humidity of around $50\% \pm 3\%$ (Figure 1). The freezing process was filmed via a high-speed camera. When the water droplet froze completely, the probe attached to the force meter approached the droplet at 0.5 mm/s , and the maximum force required to remove the frozen droplet from the sample surface was recorded. The ice adhesion strength of each sample was obtained by dividing the maximum force by the contact area of the frozen water droplet–sample interface.

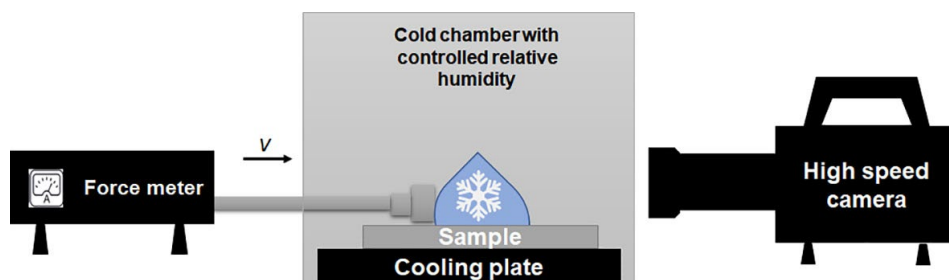


Figure 1. Schematic of micro-push-off apparatus.

Similar to the micro-push-off test, non-impact ice was used in the push-off test, but in this procedure, the ice adhesion was evaluated in a larger scale. A cylindrical plastic mold with the diameter of 1 cm was placed onto the samples while they were kept in a cold chamber at $-10.0\text{ }^{\circ}\text{C} \pm 0.2\text{ }^{\circ}\text{C}$. Then, they were filled with adequate deionized water and left in the chamber for 24 h to obtain a frozen water column. In the following day, the samples were placed on the holder of the push-off apparatus, and the maximum force for ice detachment was recorded when the probe of force meter approached the cylindrical column. The ice adhesion strengths of the samples were obtained by dividing their corresponding maximum force by the cross-sectional area of the plastic mold.

The ice accumulation on the samples was also evaluated using SAT. First, the coatings were applied to $3\text{ cm} \times 15\text{ cm}$ aluminum substrates by using a ZEHNTNER film applicator. After the curing process, they were placed onto a special-designed stand with inclined angles of 0° , 45° , and 80° and placed in a cold chamber at $-5.0\text{ }^{\circ}\text{C} \pm 0.2\text{ }^{\circ}\text{C}$ and, under relative humidity of around $84 \pm 2\%$. Then, the samples were exposed to freezing drizzle conditions by spraying supercooled water microdroplets with an average diameter of $327\text{ }\mu\text{m}$ and a temperature of $4.0\text{ }^{\circ}\text{C}$. They were iced for about 45 minutes at $-5.0\text{ }^{\circ}\text{C}$. The difference between the sample mass before and after icing condition was equaled to the amount of ice accumulated on each sample.

2.4. Durability

The durability of the samples against the subsequent de-icing events was evaluated by combining the push-off test and 20 icing/de-icing cycles. For this purpose, the ice adhesion strength of the samples after each cycle was measured.

The durability of the samples was evaluated using QUV, which included exposing to simulated outdoor circumstances. The test was conducted following the test standard of ASTM G154. The samples were exposed to about 1000 h of UV light by using UVA-340 fluorescent lamps ($0.89 \text{ W}\cdot\text{m}^{-2}$) as a test cycle of 8 h at a temperature of $60 \text{ }^\circ\text{C}$. The UV exposure was then followed by 4 h of condensation at $50 \text{ }^\circ\text{C}$.

The evaluating procedure of the replenishment capability of the samples was adopted from the work of J. Zhang et al. [47]. For this purpose, the weight of the sample was measured via a Sartorius balance (precision 0.1 mg) and recorded as m_0 . Then, the oil layer was removed from the surface using an oil-absorbing paper, and the weight of sample was again recorded. This process was repeated for n cycles, and the rate of weight loss was obtained using the Equation 1.

$$\text{Rate of weight loss} = \frac{m_0 - m_n}{m_0} \times 100 \quad \text{Equation 1}$$

Where m_n is the weight of sample after n cycles.

2.5. Electrical properties

The dielectric response of the samples at $25 \text{ }^\circ\text{C}$ was evaluated via a Novocontrol broadband dielectric spectrometer (Microtonic Alpha-A high-performance frequency analyzer). The frequency was changed from 10^{-2} Hz to 10^6 Hz . The coatings were applied using a film applicator on circular-shaped paper substrates with a diameter of 46 mm and a thickness of 2 mm. The measurement was carried out by placing the prepared samples between two solid electrodes to form a capacitor and then applying an AC voltage of 3 V.

The flashover voltage was measured via a rod-plate configuration connected to the AC voltage source. The coatings were applied to porcelain substrates and then placed between two electrodes with a fixed distance of 36 mm (Figure 2a). The test procedure was

conducted under two steps: rapid increase and gradual increase in voltage. The first step was continued until 50% of the predicted flashover value. Meanwhile, in the second step, the voltage was gradually increased at a rate of 0.5 kV/s until a disturbing discharge occurred, and then the corresponding voltage was recorded. The procedure was repeated 10 times on each sample. Furthermore, a 2-minute interval between each trial was allocated to dissipate the residual charges on the samples.

Three different conditions, namely, nonpolluted/dry, polluted/dry, and nonpolluted/wet, were chosen for each sample. A dispersion of Kaolin in deionized water was used to pollute the samples, which were then wetted by spraying deionized water on their surface before applying the voltage.

Flashover test was carried out under sub-zero and zero temperature conditions. The rod-plate configuration was transferred into an EH40-2-3 climatic chamber with adjustable temperature. Once the temperature reached $-10\text{ }^{\circ}\text{C}$, deionized water was sprayed over the samples. When water was frozen, the flashover measurement was conducted on the basis of the abovementioned procedure. The flashover voltages were also measured at $-5\text{ }^{\circ}\text{C}$ and $0\text{ }^{\circ}\text{C}$. The measurement was repeated five times for each sample, with a 2-minute interval between each event.

Condensation test was conducted in accordance with the test method proposed by the previous research work [57]. Under high-humidity condition, the moisture could be settled on the surface of cold insulator, resulting in the formation of a thin water layer. Therefore, the samples were placed in a chamber with variable temperature between $10\text{ }^{\circ}\text{C}$ and $35\text{ }^{\circ}\text{C}$ and a relative humidity of 95% (Figure 2b). For achievement of a uniform condensed water, the temperature of the chamber was increased to $35\text{ }^{\circ}\text{C}$ for 30 min, resulting in

condensation settlement on the surface. Then, the temperature was lowered to 10 °C for another 30 min. During the test, a low electric field of 4 kV/cm was applied, and the leakage current was monitored. A leakage current greater than 5 mA was considered as failure.

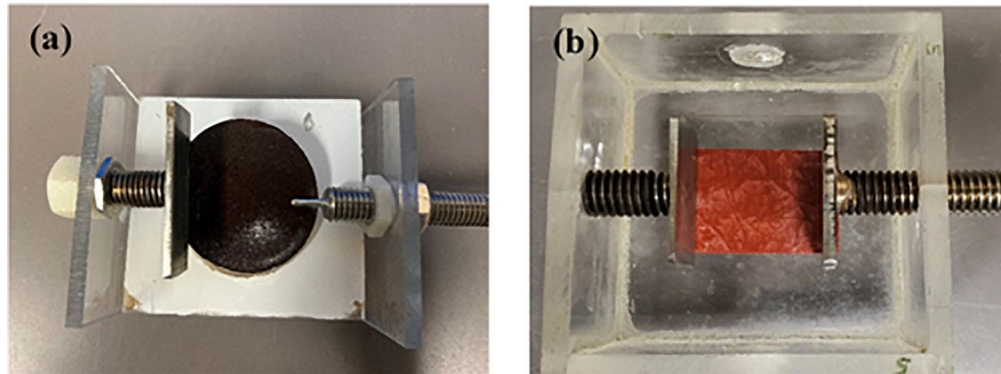


Figure 2. (a) Top view of the flashover and (b) condensation setups.

The inclines plane test (IPT) was used to assess the erosion and tracking resistance of the samples on the basis of the test standard of IEC 60587 [58]. This test is usually carried out either at constant voltage or by voltage steps. In the present work, the second process was used on the applied coatings on GPO3 substrates with standard dimensions of 50 mm width, 120 mm length, and 5.5 mm thickness and 5 mm diameter holes for fixing (Figure 3). GPO-3 is a glass reinforced thermoset polyester with excellent tracking performance, and it was used in this work because its shape could allow samples to be easily produced. The prepared samples were placed on the holder that could accommodate them at an inclination angle of 45°. The contaminant consisted of an electrolyte solution of 0.1 wt.% NH₄Cl and 0.02 wt.% Triton X100 in deionized water. Once the contaminant solution was flowing evenly at a rate of 0.6 mL/min through the filter, an initial 60 Hz of high voltage

was applied, followed by 2.5, 3, and 3.5 kV (each for 45 min). The carbonaceous path (track) produced on the samples due to the arcing was used to analyse the tracking and erosion lines of the samples. Moreover, a thermal camera was used to evaluate the leakage current and the variation of temperature. The endpoint was determined when the leakage current passing through the sample exceeded 60 mA.

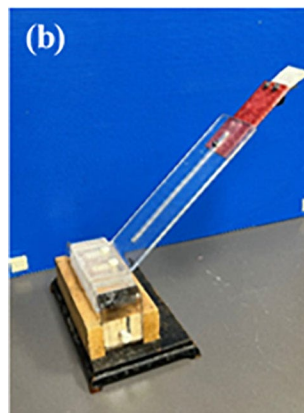
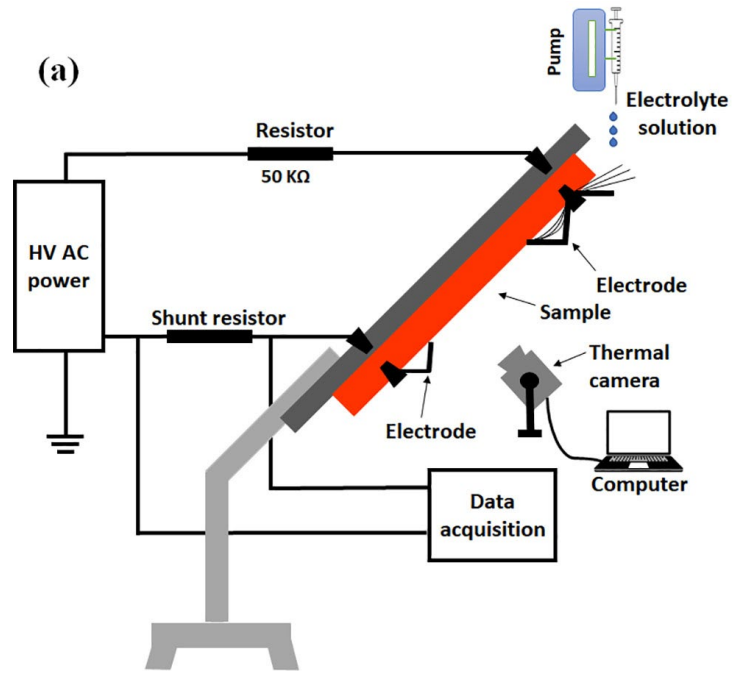


Figure 3. (a) Schematic illustrating the test setup for inclined plane test (IPT); (b) and (c) parts used for mounting the samples for IPT.

3. Results and discussion

3.1. Surface characterization

The water contact angle was measured to assess the effect of impregnating lubricant-loaded carriers on the coating wettability (Figure 4). Increasing the carrier content from 5 wt.% to 15 wt.% resulted in the contact angle decreasing from 105° for the reference to 93° (LLC-5), 90° (LLC-10), and 88° (LLC-15), respectively. In general, incorporating the carriers could result in reduced contact angle due to the lower surface energy of oil than that of the matrix. However, the variation of lubricant-loaded carrier content did not significantly affect the contact angle and the wettability of the samples containing the carriers. Water contact angle hysteresis also decreased by heightened carrier concentrations. In fact, reduced contact angle hysteresis equaled to decreased pinning points between the water droplet and the surface and consequently, easy removal of the water droplet (see Video S1). The topographical maps of the samples and their corresponding surface roughness values were obtained by profilometry (Figure 5). Accordingly, impregnating the lubricant-loaded carriers increased the surface roughness from 126 nm to 319 nm, very likely due to the presence of aerogel in the coating structure.

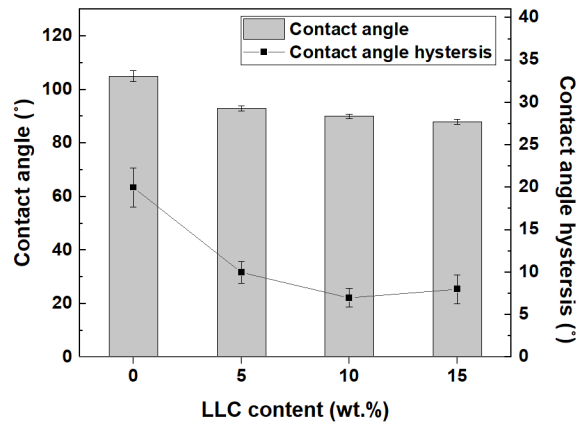


Figure 4. Variation of contact angle and contact angle hysteresis as a function of LLC content.

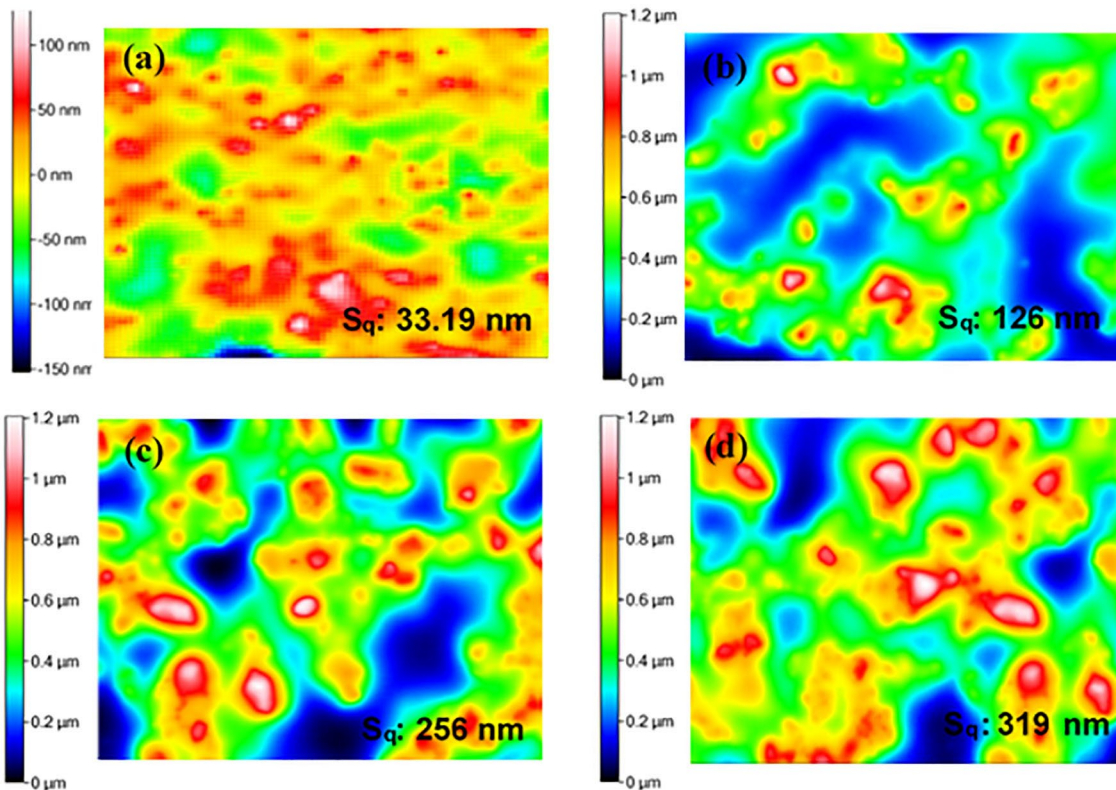


Figure 5. 3D topographical maps of the (a) reference and LLC-5, (b) LLC-10, and (c) LLC-15.

3.2. Icephobicity

The icephobic characteristics of prepared coatings are usually evaluated using two different groups of methods. The test methods, such as measuring ice nucleation temperature, belong to the first group that characterize the samples before freezing. The latter ones, including ice adhesion measurement and SAT, are related to the performance of the samples in removing ice from the surface.

The ice nucleation temperature corresponding to each sample was evaluated using DSC. As seen in Figure 6a, the ice nucleation temperature continuously decreased from $-16.25\text{ }^{\circ}\text{C}$ for the reference to $-23.53\text{ }^{\circ}\text{C}$ for the sample containing 15% of the lubricant-loaded carriers. The reduced ice nucleation time could be related to the decreased thermal conductivity of the coating due to the presence of the lubricant. In general, the thermal conductivity of silicone oils is lower than that of the PDMS matrix. Therefore, adding the lubricant to the matrix could result in the increased heat insulation effect of the coating system and consequently, delayed ice nucleation temperature. A notable detail that even a decrease of $1\text{ }^{\circ}\text{C}$ in ice nucleation temperature could lead to multifold increase in ice nucleation rate [59].

The de-icing performance of the prepared coating was evaluated using SAT method, which exhibited the amount of ice accumulated on the samples inclined at 0° , 45° , and 80° (Figure 6b). The ice accumulation on the samples decreased by impregnating lubricant-loaded carriers. Moreover, the increased carrier content resulted in a gradual reduction in accumulated ice on the surface from 12.28, 6.89, and 4.1 g for the reference to 8.36, 3.92, and 1.95 g for LLC-15 samples at their corresponding angles, respectively.

The tangential component (F_{\parallel}) of the gravity force (W) equaled to $W \cdot \sin\alpha$, (α : the inclined angle) is a key factor in removing ice from the prepared samples. Increasing the inclined angle led to greater tangential force and consequently, less ice accumulation.

Meanwhile, ice adhesion strength, as the main resisting force against ice detachment, could significantly affect the amount of ice accumulated on the surface. Micro-push off adhesion test was used to evaluate the ice adhesion strength on the samples (Figure 6c). By using water droplet, micro-push-off test aims to measure ice adhesion in a smaller scale than push-off test. Furthermore, in micro-push-off test, parameters such as humidity could be controlled more.

As illustrated in Figure 6c, adding the lubricant-loaded carriers to the coating decreased the ice adhesion strength from about 180 kPa for the reference to around 14 kPa for LLC-15 samples. The presence of oil over the surface could be the reason for the reduced ice adhesion of the samples. TGA confirmed that the loaded-lubricant mass value for the prepared powders was about 47%. This infused oil could migrate from the pores towards the surface to facilitate ice sliding. This migration occurred from the inner pores of aerogels into the large free volume of the polymeric bulk due to the produced concentration gradient pressure. The lubricant is then transferred into the surface because of the mobility of the lubricant small molecules through the bulk [51]. Another possible mechanism for the reduced ice adhesion is that the hydroxyl-terminated silicone oil had hydrophilic groups that could produce hydrogen bonding with water molecules. These hydrogen-bonded molecules could preserve water in non-frozen state at or below 0 °C, resulting in an additional factor to decrease ice adhesion [51][60].

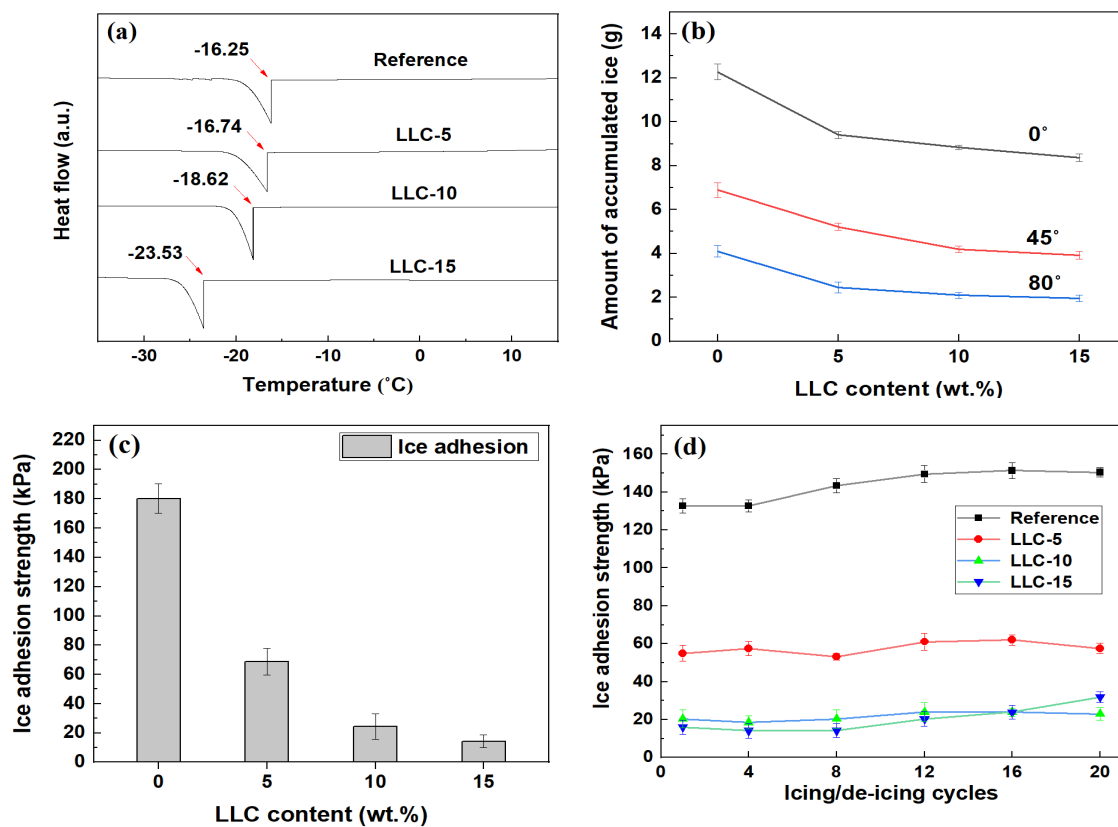


Figure 6. (a) DSC evaluation of ice nucleation temperatures corresponding to samples with LLC content. (b) Ice accumulation on samples inclined at 0°, 45°, and 80°, as measured by SAT. (c) Ice adhesion strength of samples, as obtained using micro-push-off test. (d) Ice adhesion strength in samples containing LLC over 20 icing/de-icing cycles, as obtained by push-off test.

3.3. Durability

3.3.1. Subsequent de-icing events

A total of 20 icing/de-icing cycles were conducted in the present study (Figure 6d), and the ice adhesion strength was evaluated after each four trials by using push-off adhesion test. For the LLC-5 and LLC-10 samples, no significant change was observed over all subsequent cycles, Meanwhile, for LLC-15, the ice adhesion strength increased slightly after 12 icing/de-icing cycles, very likely due to the depletion of oil on the surface, consequently increasing the surface roughness.

The presence of the micropores can promote the oil trapping within the aerogel. When the uppermost oil layer is removed from the surface, the capillary effect causes the lubricant to be transferred from the bulk towards the surface. In other words, ice detachment from the surface can eliminate the accessible oil layer, producing a concentration gradient of lubricant between the surface and the bulk that serves as a driving force for the lubricant transferring[51]. The presence of LLC results in the lubricant to be released in lower rate, and guarantees the slipperiness for longer service life. Moreover, no significant change was observed over the icing/de-icing cycles that confirmed the capability of the surface in lubricant recovery.

3.3.2. Accelerated weathering test

Exposure to weathering conditions, such as UV and humidity, could lead to deterioration of coatings. Therefore, the effect of these weathering conditions on the surface and icephobic characteristics of the fabricated coatings was investigated.

Figure 7 illustrates the evaluation of ice adhesion strength of the fabricated samples exposed to accelerated weathering conditions for 45 days, which equalled to about 5 years

of real outdoor conditions[61]. In general, the coatings containing LLC maintained their icephobic performance even after a 1000-h exposure period to UV irradiation and humidity condensation. Furthermore, increasing the LLC content in the coating could result in more durable coating under these harsh conditions. This finding could be related to further availability of the oil in higher LLC content when it migrated from bulk towards the surface. The presence of the oil layer on the surface could reduce the effect of UV light on the physical and chemical properties of the coating [62]. Thus, despite the increasing trend of ice adhesion strength for 45 days, LLC-15 maintained its ice adhesion strength to below 25 kPa. For the reference sample that had no LLC, the ice adhesion increased significantly after the exposure period.

Considering their presentation of desired icephobic characteristics and stability against weathering, LLC-10 and LLC-15 were chosen to evaluate their electrical performance in the next section.

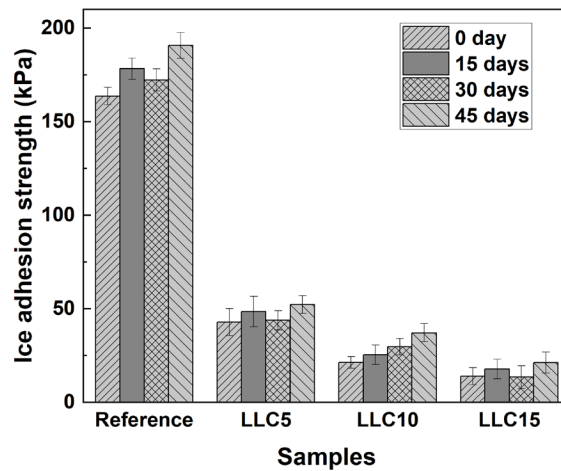


Figure 7. Evaluation of ice adhesion strength corresponding to samples during 45-day accelerated weathering test.

3.3.3. Lubricant replenishment

The lubricant depletion is considered as one of the main challenges of the slippery coatings that affects their service life. The lubricant lost of the fabricated samples was assessed over ten cycles (Figure 8). We compared the lubricant weight loss of LLC-15 and the reference (the coating containing the same amount of oil but without aerogel). It was observed that both samples show a gradual loss of lubricant over repeated cycles. Although the sample containing LLC offered much better lubricant retention properties than the reference. It can be related to using the three-step procedure that can significantly control the delivery of the lubricant on the surface, and therefore, it contributed effectively to reducing the lubricant depletion rate.

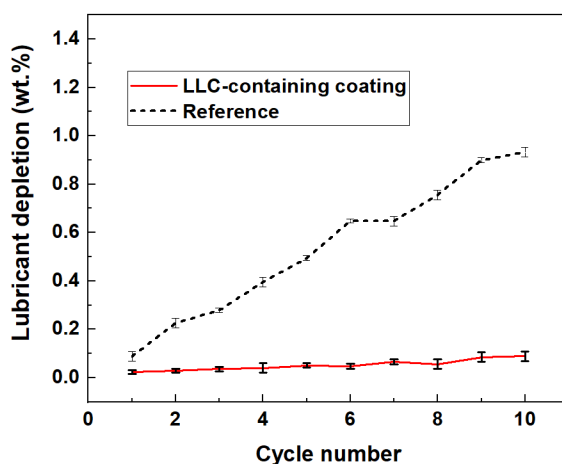


Figure 8. The rate of weight loss the coating containing LLC and the reference (the coating containing the same amount of oil but without aerogel) in relation to the number of test cycles of oil recovery/depletion.

3.4. Electrical characterization

3.4.1. Dielectric spectral analysis

Dielectrical spectroscopy is a common method to measure the permittivity and loss factor of insulating materials. In a complete insulating system, having a zero resistive leakage current ($I_R = 0$) is desirable. As this value could not be achievable, the insulation level is usually expressed by dissipation factor, $\tan \delta$, which be defined as the equation 2 [63, 64].

$$\tan \delta = \frac{|I_R|}{|I_C|} \approx \frac{\varepsilon''(\omega)}{\varepsilon'(\omega)} \quad \text{Equation 2}$$

In this equation; ε' is the real part of the permittivity related to material dissipation; ε'' is the imaginary part of permittivity, which is equal to polarization losses; and I_R and I_C are the resistive and capacitive currents, respectively. Accordingly, a dissipation factor as small as possible must be achieved.

Figure 9 depicts the variation of ε' , ε'' , and the dissipation factor ($\tan \delta$). From the graphs, at low frequency, ε' and ε'' showed increased values, which then dropped dramatically when the frequency was increased and then levelled out with the change to high frequencies. In fact, the dipoles could become readily oriented with the electrical field at lower frequencies, resulting in enhanced mobility of the segments and consequently, increased values of ε' and ε'' . The high values of ε' and ε'' could be attributed to conductivity and polarization losses, respectively. Meanwhile, at higher frequencies, the dipoles are not able to reorient rapidly with the electrical field due to lack of enough time.

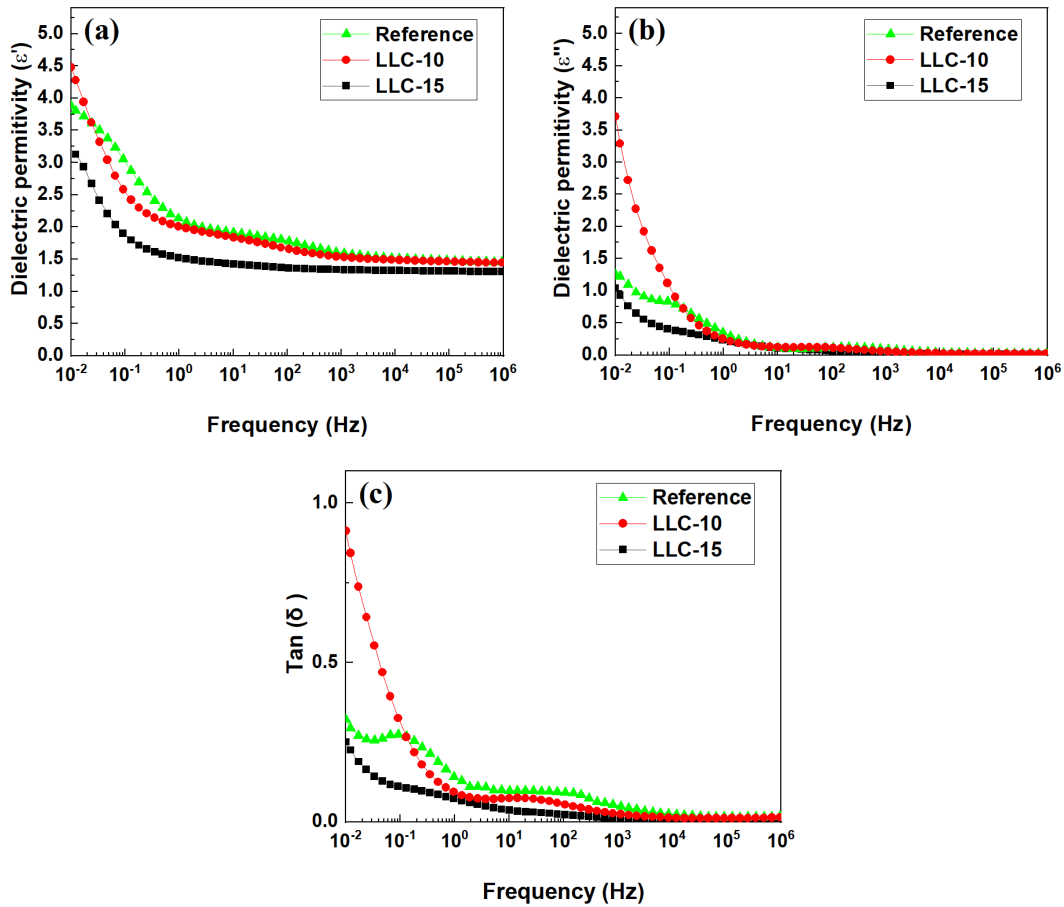


Figure 9. Variation of (a) real (ϵ') and (b) imaginary (ϵ'') parts of permittivity and (c) dissipation factor ($\tan \delta$) in relation to frequency.

As illustrated in Figure 9a and Figure 9b, the ϵ' and ϵ'' values of the prepared coating were lower than those of the reference. Silicone oils are generally considered as nonpolar liquids with a low dielectric constant and loss factor and high electrical resistivity [65–67]. These liquids also offer low temperature and frequency dependency of electrical constant and dissipation factor [68]. Infusing silicone oil within the elastomeric matrix reduced the

number of dipoles within coatings, resulting in reduced total dielectric constant and increased resistivity compared with reference samples.

Figure 9c illustrates the variation of $\tan \delta$ in terms of frequency at 25 °C. This factor obviously decreased rapidly by increasing the frequency and stabilized in high frequencies. The insulating properties of the lubricant infused within the matrix could prevent the electron mobility throughout the prepared coating at high frequencies. Moreover, LLC-15 showed the best performance in terms of $\tan \delta$ at a power frequency of 60 Hz.

3.4.2. Flashover

High-voltage test is one of the essential techniques to evaluate the electrical performance of insulators by monitoring the flashover voltage of coated and uncoated surfaces. In this method, the maximum tolerance of surfaces is evaluated under applying high-voltage stress on a 36 mm sample. Figures 9a–9c illustrate the variation of flashover levels for the fabricated slippery coatings and uncoated surfaces in different conditions, including clean/dry, polluted/dry, and polluted/wet states.

Under the clean/dry condition, the slippery coatings of LLC-10 and LLC-15 showed a disruptive discharge at around 35 kV, and LLC-15 could remain at this level after 10 repeated tests (Figure 10a). For the polluted condition in dry state (Figure 10b), the presence of pollution had no high negative effect on the performance of the coating under high voltage stress, and the coated surface could tolerance the same level of flashover (35 kV) as dry state, with acceptable stability after repetitive test. However, for the polluted/wet state (Figure 10c), a different behavior was observed between the slippery coatings containing LLC and the reference coating while water was sprayed. The slippery coatings did not allow the water to remain over the surface because of their slippage

properties, whereas the reference coating did not have such characteristic, and the water film spread over the surface and completely wetted it. Therefore, the flashover level for reference (under 25 kV) was considerably lower than that for the fabricated coatings. After repeated cycles, the reference coating underwent electrical discharge, and the level of flashover dropped to about 15kV. The results indicated that the insulation effect of slippery coatings containing LLC not only degraded the electrical performance of the surface but also made it more stable against electrical discharge and flashover.

Figure 10d illustrates the evaluation of the flashover voltage at $-10\text{ }^{\circ}\text{C}$, $-5\text{ }^{\circ}\text{C}$, and $0\text{ }^{\circ}\text{C}$. At $-10\text{ }^{\circ}\text{C}$, the samples generally showed the highest flashover voltages, and upon increasing the temperature, a reducing trend was observed for all samples. Increasing the LLC content resulted in increased flashover voltage at all temperatures. Furthermore, for $0\text{ }^{\circ}\text{C}$, at which ice turned into water, the difference between the flashover voltages corresponding to the reference sample and LLC-10 was higher than those at $-10\text{ }^{\circ}\text{C}$ and $-5\text{ }^{\circ}\text{C}$. This finding could be related to the presence of a lower amount of water on the coatings containing LLC, which resulted from the slippage property of the coatings.

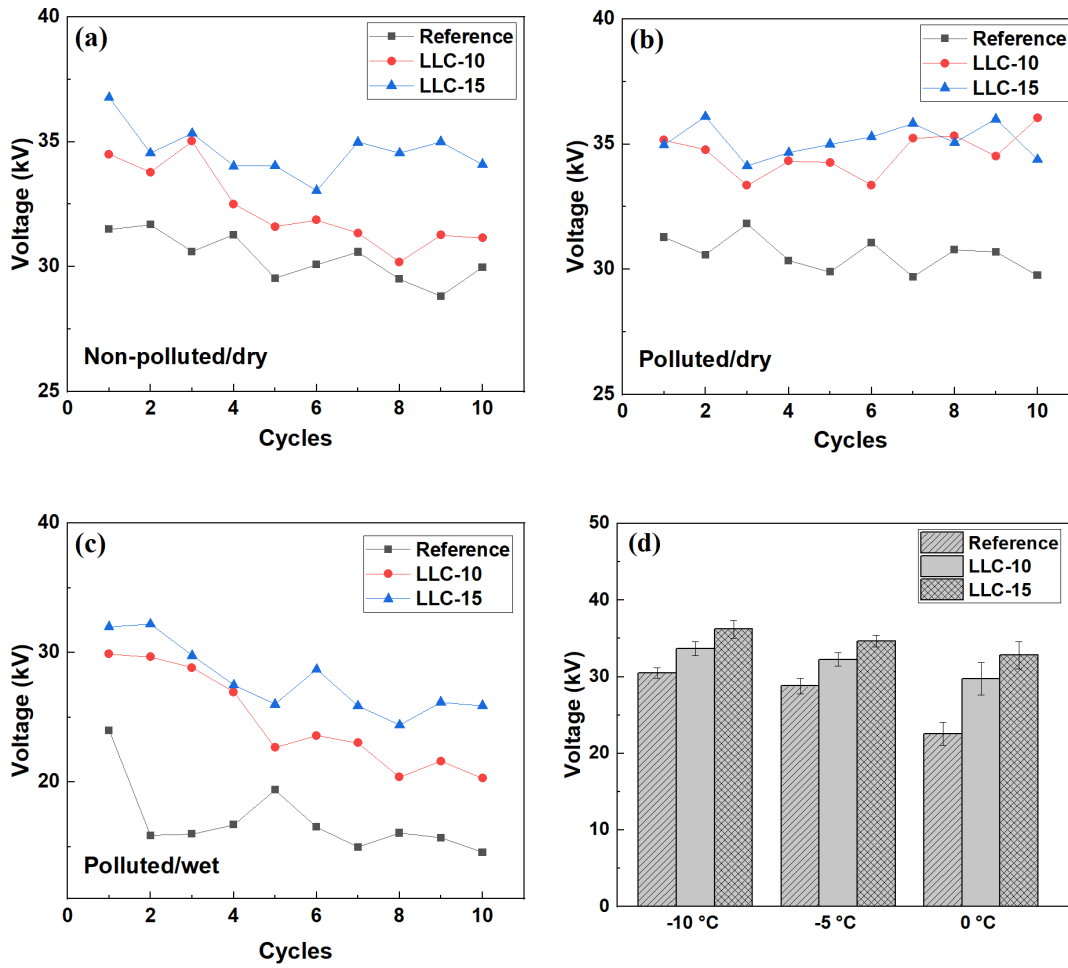


Figure 10. Evaluation of flashover voltage during 10 subsequent cycles under (a) non-polluted/dry, (b) polluted/dry, and (c) polluted/wetted conditions. (d) Evaluation of first flashover voltage at $-10\text{ }^{\circ}\text{C}$, $-5\text{ }^{\circ}\text{C}$, and $0\text{ }^{\circ}\text{C}$.

3.4.3. Condensation test

Condensation test was conducted to evaluate the electrical performance of the prepared coatings under controlled humidity conditions [57]. Figure 11a and Figure 11b exhibits the variation in leakage current for three cycles and the three-cycle average leakage current

during subsequent heating/cooling events. The first smaller cycle (0–40 min) is a preliminary test to carry out the subsequent tests under the same initial conditions. Increasing the LLC content led to decreased leakage current. The leakage current of LLC-15 samples dropped to around 0.02 mA, whereas for GPO3, the leakage current was 0.26 mA in wet state (0–30 min). Thus, the presence of lubricant in the coating enhanced the electrical insulation of the coatings and subsequently, the leakage current decreased considerably.

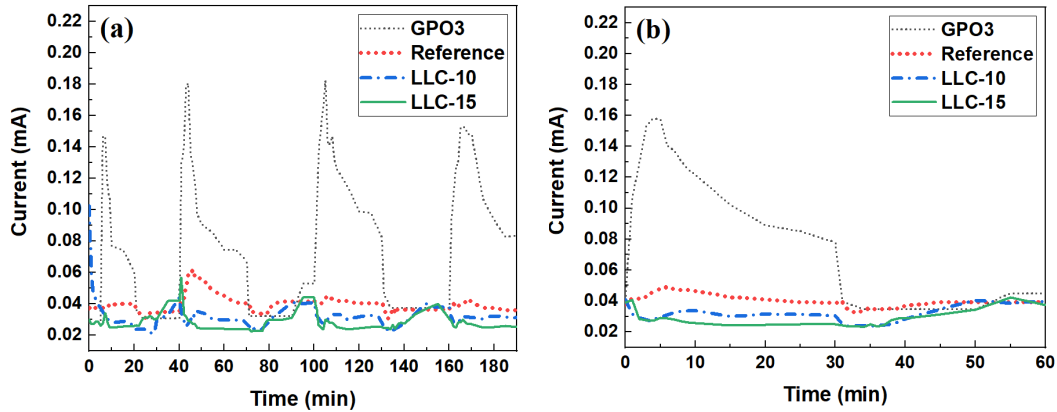


Figure 11. Evaluation of leakage current versus time on samples for a) three repetitive cycles and b) their averages, as obtained by condensation test.

3.4.4. Inclined plane test (IPT)

IPT is used to evaluate the resistance of slippery coatings against tracking and erosion when they are exposed to electrical voltage [58]. First, the contamination solution was continuously flowed over the surface, and then the voltage was applied, resulting in leakage current. Consequently, this leakage current caused the erosion and tracking of the material over the surface due to the enhanced possibility of electrical discharge. Figure 12a illustrates the thermal camera images of the samples at the final step of IPT. In these images,

the bright yellow arcs corresponded to the erosion of the surfaces. Accordingly, for samples containing LLC, such arcs spread in a narrower area than that for the reference. Figure 12b and Figure 12c shows the samples' surfaces after the test, in which the eroded area and tracking path were clearly visible. Accordingly, the tracks and cracks on the pristine surface were wider and deeper than those on the samples containing LLC. This finding could be related to the slippage of water droplet on the sample containing lubricant, which enhanced the water droplet velocity over them, resulting in reduced polluted spots that contributed to the initiation and progress of erosion. Figure 11d illustrates the leakage current evolution of the slippery coatings of LLC-10, LLC-15, and reference surface. The leakage current trend of each step showed various behavior for the corresponding sample. In the first step (2.5 kV), the reference sample exhibited the highest level of leakage current at around 8 mA. Meanwhile, the leakage current of the fabricated coatings was about 4 mA. By increasing the voltage in the next step (3 kV), the leakage current increased for all the samples. However, the LLC-15 sample showed a little bit higher level of leakage than the LLC-10 sample. This behavior confirmed that the coating containing a lower content of lubricant-loaded porous particles exhibited, to some extent, more resistance towards degradation under applied voltage over time. Moreover, it could keep such a low leakage current even until the final step with a high level of voltage (3.5 kV). However, both slippery coatings generally did not allow the leakage current to increase significantly under high-voltage level. Moreover, considering that IPT is a very harsh test, the slippery coatings showed promising performance against tracking and erosion for electrical application.

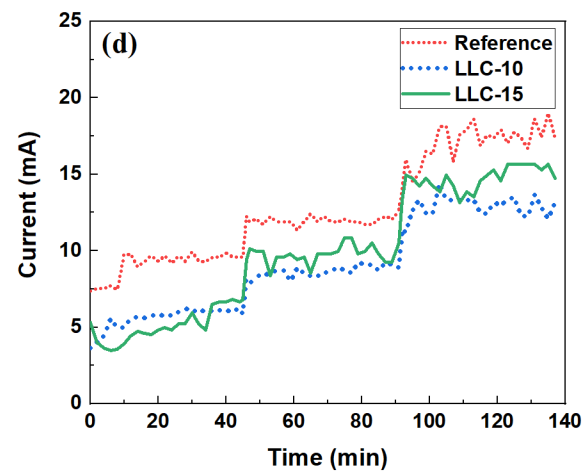
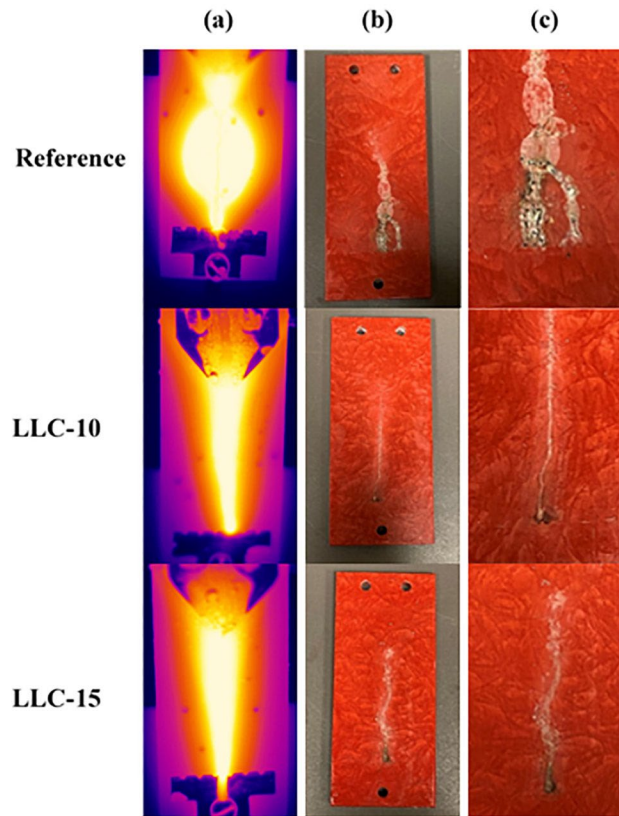


Figure 12. (a) Thermal camera images of samples at the final minutes of IPT. (b) and (c) Images of the samples after the test. (d) Evaluation of leakage current over time during IPT.

4. Conclusion

Scalable slippery coatings were designed by impregnating lubricant-loaded carriers into a silicone-based blend. The lubricant-loaded carriers were obtained through a three-step procedure by applying negative pressure to enhance the infusing oil within the aerogel's pores. The icephobic and electrical properties of the coatings with various carrier contents were evaluated to obtain an optimized formulation. Using hydroxyterminated silicone oil as a lubricant could promote the production of nonfrozen hydrogen-bonded molecules, which probably contributed to the enhancement of icephobic properties. The coatings containing lubricant-loaded carriers showed acceptable resistance against weathering conditions, including harsh condensation cycles and UV exposure. The electrical properties of the coatings were also assessed using a comprehensive set of test methods under various conditions.

The coatings exhibited decreased dielectric permittivity and loss factor under applied frequency range of 10^{-4} – 10^3 Hz, very likely due to the nonpolar characteristics of the infused lubricant. Furthermore, due to the insulating effect of the fabricated coatings, they had desirable resistance against electrical discharge and flashover voltage, particularly under wet and polluted conditions. The condensation test also confirmed that the coatings enhanced the insulation performance of the insulators under controlled high-humidity circumstances. The adapted was carried out to evaluate the erosion and tracking resistance of the samples under applied voltage steps. The results confirmed that the coatings with

lubricant-loaded-carriers were more resistant against the degradation caused by applied voltage over time, and they preserved a low leakage current even under a high voltage of 3.5 kV.

In summary, the coating containing LLC exhibited desirable anti-icing and electrical performance that opens an avenue towards designing efficient strategies to tackle icing-related challenges on high-voltage insulators.

Acknowledgement

The authors acknowledge all support from the Natural Sciences and Engineering Research Council of Canada (NSERC), Hydro-Québec, and PRIMA Quebec. The authors would like to thank CENGIVRE for providing the icing infrastructure and Ms Caroline Blackburn at the Anti-icing Materials International Laboratory (AMIL), UQAC, for helping carry out the SAT test. They also would like to give very special thanks to Frederick Munger for performing the high voltage tests.

Author contributions

Samaneh Heydarian: Conceptualization, Methodology, Investigation, Formal analysis and experiment performing, Planning and results interpretation, Visualization , Writing – original draft, Writing – review & editing. **Gelareh Momen:** Conceptualization, Supervision, Resources, Writing – review & editing, Project administration, Funding acquisition. **Reza Jafari:** Conceptualization, Supervision, Resources, Writing – review & editing.

Conflicts of interest

The authors declare that they have no known competing financial interests or personal relationships that could have appeared to influence the work reported in this paper.

Data and code availability

Not Applicable.

Supplementary information

Not Applicable.

Ethical approval:

Not Applicable.

5. References

1. Xu J, Yin F, Li L, et al (2019) Wet snow flashover characteristics of 500-kV AC insulator strings with different arrangements. *Appl Sci* 9:930.
<https://doi.org/10.3390/app9050930>
2. Zong C, Hu Y, Jiang X, et al (2022) AC flashover characteristics and arc development process of glaze ice-covered insulators in natural environment. *Int J Electr Power Energy Syst* 135: 107559.
<https://doi.org/10.1016/j.ijepes.2021.107559>
3. Farzaneh M (2014) Insulator flashover under icing conditions. *IEEE Trans Dielectr Electr Insul* 21:1997–2011. <https://doi.org/10.1109/TDEI.2014.004598>
4. Sanyal S, Aslam F, Kim T, et al (2020) Deterioration of Porcelain Insulators Utilized in Overhead Transmission Lines: A Review. *Trans. Electr. Electron.*

Mater. 21:16–21

5. Hu Q, Wang S, Yang H, et al (2016) Effects of icing degree on ice growth characteristics and flashover performance of 220 kV composite insulators. *Cold Reg Sci Technol* 128:47–56. <https://doi.org/10.1016/j.coldregions.2016.04.010>
6. Jiang X, Xiang Z, Zhang Z, et al (2014) Comparison on ac icing flashover performance of porcelain, glass, and composite insulators. *Cold Reg Sci Technol* 100:1–7. <https://doi.org/10.1016/j.coldregions.2013.12.010>
7. Huang Y, Jiang X, Virk MS (2020) Study of inverted T-shape insulator strings in icing conditions. *Cold Reg Sci Technol* 173: 103021. <https://doi.org/10.1016/j.coldregions.2020.103021>
8. M. Farzaneh et al. (2015) Coatings for Protecting Overhead Power Network Equipment in Winter Conditions. *CIGRE, Electra* 283:41–45
9. Chaudhry AN, Billingham NC (2001) Characterisation and oxidative degradation of a room-temperature vulcanised poly(dimethylsiloxane) rubber. *Polym Degrad Stab* 73:505–510. [https://doi.org/10.1016/S0141-3910\(01\)00139-2](https://doi.org/10.1016/S0141-3910(01)00139-2)
10. Suwarno, Basuki A, Lendy F, Sumedi (2012) Improving outdoor insulator performances installed at coastal area using silicone rubber coating. In *Proceedings of 2012 IEEE International Conference on Condition Monitoring and Diagnosis, CMD 2012*. pp 1143–1146
11. Ahmadi-Joneidi I, Rezaei M, Kahuri H, et al (2013) Evaluation of actual field ageing on room temperature vulcanized silicone rubber coating of ceramic

insulators on 230/63 substation. *Life Sci J* 10:833–838

12. Isa M, Othman M, Abdullah AZ, et al (2019) Characteristics of RTV Coating on Ceramic Insulator. In: 2019 IEEE International Conference on Automatic Control and Intelligent Systems, I2CACIS 2019 - Proceedings. pp 114–117
13. Momen G, Farzaneh M, Jafari R (2011) Wettability behaviour of RTV silicone rubber coated on nanostructured aluminium surface. *Appl Surf Sci* 257:6489–6493. <https://doi.org/10.1016/j.apsusc.2011.02.049>
14. Ramirez I, Hernandez R, Montoya G (2012) Salt fog testing of RTV coated ceramic insulators and comparison with HTV silicone rubber insulators. In: Annual Report - Conference on Electrical Insulation and Dielectric Phenomena, CEIDP. pp 794–797
15. Siderakis K, Agoris D (2008) Performance of RTV silicone rubber coatings installed in coastal systems. *Electr Power Syst Res* 78:248–254. <https://doi.org/10.1016/j.epsr.2007.02.013>
16. Sorqvist T (2000) Long-term field experience with RTV coated porcelain insulators. In: Conference Record of IEEE International Symposium on Electrical Insulation. pp 201–206
17. Shamshiri M, Jafari R, Momen G (2021) Potential use of smart coatings for icephobic applications: A review. *Surf Coatings Technol* 424:127656. <https://doi.org/10.1016/j.surfcoat.2021.127656>
18. Yassin AY, Mohamed AR, Abdelghany AM, Abdelrazek EM (2018) Enhancement

of dielectric properties and AC electrical conductivity of nanocomposite using poly (vinyl chloride-co-vinyl acetate-co-2-hydroxypropyl acrylate) filled with graphene oxide. *J Mater Sci Mater Electron* 29:15931–15945.

<https://doi.org/10.1007/s10854-018-9679-7>

19. Qiao X, Zhang Z, Jiang X, et al (2020) AC failure voltage of iced and contaminated composite insulators in different natural environments. *Int J Electr Power Energy Syst* 120: 105993. <https://doi.org/10.1016/j.ijepes.2020.105993>
20. Wei X, Jia Z, Sun Z, et al (2012) Study of anti-icing performance of insulator strings bottom-coated with semiconductive silicone rubber coating. *IEEE Trans Dielectr Electr Insul* 19:2063–2072. <https://doi.org/10.1109/TDEI.2012.6396966>
21. Momen G, Farzaneh M (2010) Study of ice accumulation on nanocomposite semiconducting coatings. In: *Annual Report - Conference on Electrical Insulation and Dielectric Phenomena, CEIDP, USA, 2010*, pp. 1-4, [10.1109/CEIDP.2010.5724058](https://doi.org/10.1109/CEIDP.2010.5724058).
22. Taghvaei M, Sedighizadeh M, NayebPashae N, Sheikhi Fini A (2020) Thermal stability of nano RTV vs. RTV coatings in porcelain insulators. *Therm Sci Eng Prog* 20:100696. <https://doi.org/10.1016/j.tsep.2020.100696>
23. Cherney E, Marzinotto M, Gorur R, et al (2014) End-of-life and replacement strategies for RTV silicone rubber coatings. *IEEE Trans Dielectr Electr Insul* 21:253–261. <https://doi.org/10.1109/TDEI.2013.004185>
24. Taghvaei M, Sedighizadeh M, NayebPashae N, Fini AS (2021) Reliability assessment of RTV and nano-RTV-coated insulators concerning contamination

- severity. *Electr Power Syst Res* 191: 106892.
<https://doi.org/10.1016/j.epsr.2020.106892>
25. Allahdini A, Momen G, Munger F, et al (2022) Performance of a nanotextured superhydrophobic coating developed for high-voltage outdoor porcelain insulators. *Colloids Surfaces A Physicochem Eng Asp* 649:129461.
<https://doi.org/10.1016/J.COLSURFA.2022.129461>
26. Arshad, Momen G, Farzaneh M, Nekahi A (2017) Properties and applications of superhydrophobic coatings in high voltage outdoor insulation: A review. *IEEE Trans Dielectr Electr Insul* 24:3630–3646.
<https://doi.org/10.1109/TDEI.2017.006725>
27. Li J, Zhao Y, Hu J, et al (2012) Anti-icing performance of a superhydrophobic PDMS/modified nano-silica hybrid coating for insulators. *J Adhes Sci Technol*.9: 771,<https://doi.org/10.1163/016942411X574826>
28. Xu S, Wang Q, Wang N (2021) Chemical Fabrication Strategies for Achieving Bioinspired Superhydrophobic Surfaces with Micro and Nanostructures: A Review. *Adv. Eng. Mater.* 23: 2001083
29. Zeng Q, Zhou H, Huang J, Guo Z (2021) Review on the recent development of durable superhydrophobic materials for practical applications. *Nanoscale* 13:11734–11764
30. Quan YY, Chen Z, Lai Y, et al (2021) Recent advances in fabricating durable superhydrophobic surfaces: A review in the aspects of structures and materials. *Mater. Chem. Front.* 5:1655–1682

31. Erbil HY (2020) Practical Applications of Superhydrophobic Materials and Coatings: Problems and Perspectives. *Langmuir* 36:2493–2509.
<https://doi.org/10.1021/acs.langmuir.9b03908>
32. Allahdini A, Jafari R, Momen G (2022) Transparent non-fluorinated superhydrophobic coating with enhanced anti-icing performance. *Prog Org Coatings* 165:106758. <https://doi.org/10.1016/j.porgcoat.2022.106758>
33. de Santos H, Sanz-Bobi M (2021) Research on the pollution performance and degradation of superhydrophobic nano-coatings for toughened glass insulators. *Electr Power Syst Res* 191:. <https://doi.org/10.1016/j.epsr.2020.106863>
34. Kim P, Wong TS, Alvarenga J, et al (2012) Liquid-infused nanostructured surfaces with extreme anti-ice and anti-frost performance. *ACS Nano* 6:6569–6577.
<https://doi.org/10.1021/nn302310q>
35. Wang C, Guo Z (2020) A comparison between superhydrophobic surfaces (SHS) and slippery liquid-infused porous surfaces (SLIPS) in application. *Nanoscale* 12:22398–22424. <https://doi.org/10.1039/d0nr06009g>
36. Prakash CGJ, Prasanth R (2020) Recent trends in fabrication of nepenthes inspired SLIPs: Design strategies for self-healing efficient anti-icing surfaces. *Surfaces and Interfaces* 21:100678.
37. Li J, Ueda E, Paulssen D, Levkin PA (2019) Slippery Lubricant-Infused Surfaces: Properties and Emerging Applications. *Adv Funct Mater* 29: 1802317.<https://doi.org/10.1002/adfm.201802317>

38. Samaha MA, Gad-el-Hak M (2014) Polymeric slippery coatings: Nature and applications. *Polymers* 6:1266-1311.
39. Yao W, Wu L, Sun L, et al (2022) Recent developments in slippery liquid-infused porous surface. *Prog. Org. Coatings* 166: 106806.
40. Villegas M, Zhang Y, Abu Jarad N, et al (2019) Liquid-Infused Surfaces: A Review of Theory, Design, and Applications. *ACS Nano* 13:8517–8536, <https://doi.org/10.1021/acsnano.9b04129>
41. Okada I, Shiratori S (2014) High-transparency, self-standable Gel-SLIPS fabricated by a facile nanoscale phase separation. *ACS Appl Mater Interfaces* 6:1502–1508, <https://doi.org/10.1021/am404077h>
42. Shamshiri M, Jafari R, Momen G (2021) Icephobic properties of aqueous self-lubricating coatings containing PEG-PDMS copolymers. *Prog Org Coatings* 161:106466. <https://doi.org/10.1016/j.porgcoat.2021.106466>
43. Heydarian S, Jafari R, Momen G (2021) Recent progress in the anti-icing performance of slippery liquid-infused surfaces. *Prog Org Coatings* 151:106096. <https://doi.org/10.1016/j.porgcoat.2020.106096>
44. Latthe SS, Sutar RS, Bhosale AK, Nagappan S (2019) Recent developments in air-trapped superhydrophobic and liquid-infused slippery surfaces for anti-icing application. *Prog Org Coatings* 137:105373. <https://doi.org/10.1016/j.porgcoat.2019.105373>
45. Zeng X, Guo Z, Liu W (2021) Recent advances in slippery liquid-infused surfaces

- with unique properties inspired by nature. *Bio-Design Manuf.* 4:506–525
46. Wang X, Huang J, Guo Z (2022) Overview of the development of slippery surfaces: Lubricants from presence to absence. *Adv. Colloid Interface Sci.* 301:102602.
 47. Zhang J, Liu B, Tian Y, et al (2020) Facile one-step method to fabricate a slippery lubricant-infused surface (lis) with self-replenishment properties for anti-icing applications. *Coatings* 10: 109. <https://doi.org/10.3390/coatings10020119>
 48. Golovin K, Kobaku SPR, Lee DH, et al (2016) Designing durable icephobic surfaces. *Sci Adv* 2:1501496. <https://doi.org/10.1126/sciadv.1501496>
 49. Golovin K, Tuteja A (2017) A predictive framework for the design and fabrication of icephobic polymers. *Sci Adv* 3:1701617. <https://doi.org/10.1126/sciadv.1701617>
 50. Wang Y, Yao X, Chen J, et al (2015) Organogel as durable anti-icing coatings. *Sci China Mater* 58:559–565. <https://doi.org/10.1007/s40843-015-0069-7>
 51. Zhu L, Xue J, Wang Y, et al (2013) Ice-phobic coatings based on silicon-oil-infused polydimethylsiloxane. *ACS Appl Mater Interfaces* 5:4053–4062. <https://doi.org/10.1021/am400704z>
 52. Olad A, Maryami F, Mirmohseni A, Shayegani-Akmal AA (2021) Potential of slippery liquid infused porous surface coatings as flashover inhibitors on porcelain insulators in icing, contaminated, and harsh environments. *Prog Org Coatings* 151: 106082. <https://doi.org/10.1016/j.porgcoat.2020.106082>

53. Peppou-Chapman S, Hong JK, Waterhouse A, Neto C (2020) Life and death of liquid-infused surfaces: a review on the choice, analysis and fate of the infused liquid layer. *Chem Soc Rev* 49:3688–3715. <https://doi.org/10.1039/D0CS00036A>
54. Heydarian S, Maghsoudi K, Jafari R, et al (2022) Fabrication of Liquid-Infused Textured Surfaces (Lits): The Effect of Surface Textures on Anti-Icing Properties and Durability. *Mater Today Commun* 32:103935. <https://doi.org/10.1016/j.mtcomm.2022.103935>
55. Aghdam AS, Cebeci FC (2020) Tailoring the Icephobic Performance of Slippery Liquid-Infused Porous Surfaces through the LbL Method. *Langmuir* 36:14145–14154. <https://doi.org/10.1021/acs.langmuir.0c02873>
56. Zhou L, Liu H, Liu A, et al (2022) Easily fabricated icephobic surface with external and self-replenishing properties. *Appl Surf Sci* 579:152069. <https://doi.org/10.1016/j.apsusc.2021.152069>
57. Wu J, Schnettler A (2008) Degradation assessment of nanostructured superhydrophobic insulating surfaces using multi-stress methods. *IEEE Trans Dielectr Electr Insul* 15:73–80. <https://doi.org/10.1109/T-DEI.2008.4446738>
58. Krivda A, Schmidt LE, Kornmann X, et al (2009) Inclined-Plane Tracking and Erosion Test According to the IEC 60587 Standard. *IEEE Electr Insul Mag* 25:14–22. <https://doi.org/10.1109/MEI.2009.5313706>
59. Amirfazli A, Antonini C (2016) Fundamentals of Anti- Icing Surfaces. In: *Non-wettable Surfaces: Theory, Preparation and Applications*. Non-wettable Surfaces. Royal Society of Chemistry, p 319–346

60. Mahani AA, Motahari S, Mohebbi A (2018) Sol-gel derived flexible silica aerogel as selective adsorbent for water decontamination from crude oil. *Mar Pollut Bull* 129:438–447. <https://doi.org/10.1016/j.marpolbul.2017.10.012>
61. Maghsoudi K, Vazirinasab E, Momen G, Jafari R (2021) Icephobicity and durability assessment of superhydrophobic surfaces: The role of surface roughness and the ice adhesion measurement technique. *J Mater Process Technol* 276:116415. <https://doi.org/10.1016/j.jmatprotec.2020.116883>
62. Ullah I, Amin M, Hussain H, Nazir MT (2022) Impact of Accelerated Ultraviolet Weathering on Polymeric Composite Insulators Under High Voltage DC Stress. *J Power Energy Syst* 8:922–932. <https://doi.org/10.17775/CSEEJPES.2020.01900>
63. Latif I, B. Alwan T, H. Al-Dujaili A (2013) Low Frequency Dielectric Study of PAPA-PVA-GR Nanocomposites. *Nanosci Nanotechnol* 2:190–200. <https://doi.org/10.5923/j.nn.20120206.07>
64. Gubanski SM, Boss P, Cseépes G, et al (2003) Dielectric response methods for diagnostics of power transformers. *IEEE Electr Insul Mag* 19:12–18. <https://doi.org/10.1109/MEI.2003.1203017>
65. Hakim RM, Olivier RG, St-Onge H (1977) The Dielectric Properties of Silicone Fluids. *IEEE Trans Electr Insul* EI-12:360–370. <https://doi.org/10.1109/TEI.1977.298043>
66. Teranishi T, Ohashi A, Ueda M (1975) Dielectric Characteristics of Silicone Oils in Low Temperature Regions. *IEEJ Trans Fundam Mater* 95:118–124. <https://doi.org/10.1541/ieejfms1972.95.118>

67. Betie A, Meghnefi F, Fofana I, et al (2015) Neural network approach to separate aging and moisture from the dielectric response of oil impregnated paper insulation. *IEEE Trans Dielectr Electr Insul* 22:2176–2184.
<https://doi.org/10.1109/TDEI.2015.004731>

68. Teranishi T, Ohashi A, Ueda M (1975) Dielectric characteristics of silicone oils at low temperature. *Electr Eng Japan* 95:118–124.
<https://doi.org/10.1002/ej.4390950201>